Density Functional Theory Study of the Conductivity of the Biphenalenyl Radical Dimer

By

Aiyan Lu

B.S. Chemistry
Rutgers University, 2004

SUBMITTED TO THE DEPARTMENT OF CHEMISTRY IN PARTIAL
FULFUILLMENT OF THE REQUIREMENTS FOR THE DEGREE OF

MASTER OF SCIENCE IN CHEMISTRY
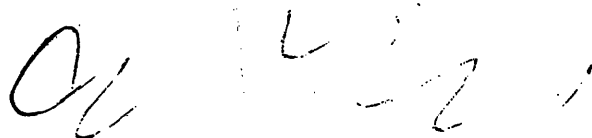AT THE
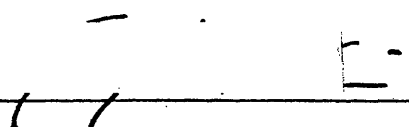MASSACHUSETTS INSTITUE OF TECHNOLOGY

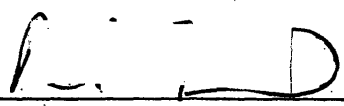APRIL 2007
[June 2007]

Signature of Author: _____
Department of Chemistry
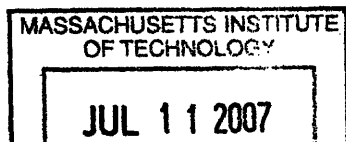April 2, 2007

Certified by: _____
Troy Van Voorhis
Assistant Professor of Chemistry
Thesis Supervisor

Accepted by: _____
Robert W. Field
Professor of Chemistry
Chairman, Committee for Graduate Students

1

Density Functional Theory Study of the Conductivity of the Biphenalenyl Radical Dimer

By

Aiyan Lu

Submitted to the Department of Chemistry
on April 1, 2007 in Partial Fulfillment of the
requirement for the Degree of Master of Science in
Chemistry

ABSTRACT

We present *ab initio* molecular calculations at different levels of density functional theory (DFT) for the spiro-biphenalenyl neurtral radical in its singlet and triplet states. We performed calculations on the dimer to study its conductivity by investigating the ground state energy, HOMO-LUMO gap, charge localization, and reorganization energies, as these are the main contributing factors to crystal conduction. We find that there is only a slight difference between the singlet state and triplet state HOMO-LUMO gaps. In addition, the negative charge spreads throughout both the interior and exterior units of the molecule in both the singlet state and the triplet state, this is in disagreement with the original argument that the conducting diamagnetic state is a result of the migration of the unpaired electrons to the interior units of the molecule. Finally, we find that the triplet state has higher reorganization energy than that of the singlet. Thus, if conduction were assumed to proceed via a hopping mechanism, the experimental observations would be explained.

Thesis Supervisor: Troy Van Voorhis
Title: Assistant Professor of Chemistry

Contents

1 Introduction

The spiro-biphenalenyl radical dimer is a molecular conductor that simultaneously exhibits bistabilities in eletrical, optical, and magnetic channels. Each biphenalenyl radical consists of two phenalenyl ring systems, spiro-conjugated through a boron atom (Fig. 2), so that the two units of the radical molecule are orthogonal to each other. Their molecular crystals display diverse physical properties. These multifunctional crystals have the potential to play a central role in the development of new types of electronic devices, where multiple physical channels are essential for reading, writing, and transfering information. In addition, the intriguing idea of molecular metals is based on neutral π-radicals [3]. In search of an intrinsic organic molecular metal, Haddon group has recently synthesized by far the best candidate, cyclohexyl-substituted biphenalenyl radical [32], see Fig 1. Surprisingly, the conductivity of the molecule increases by two orders of magnitude at the phase transition from paramagnetic state to diagmagnetic state [25]. Various conducting pathways of this spiro-biphenalenyl neutral radical molecular crystals have been proposed [24, 28, 38]. For example, Huang and Kertesz have suggested that a different band becomes the conduction band due to a spin crossover at the phase transition. Their calculation indicates that the energy gap (E_g) increases from 0.12 eV of the low-temperature (diamagnetic) polymorph to 0.23 eV of the high-temperature (paramagnetic) polymorph because it corresponds to a different occupancy causing a change in the number of available charge carriers, explaining the change of conductivity by two or-

ders of magnitude. However, a more lucid conduction mechanism remains open to discussion. More detailed understanding of the electrical property will require further experimental and theoretical work. Here, we aim to elucidate the origin of conducting diamagnetic state and insulating paramagnetic state of the biphenalenyl dimer using *ab initio* calculations.

A number of factors including ground state energies, binding energies, HOMO-LUMO gaps, and charge localizations are known to play important roles in dictating the conduction properties of conjugated organic polymers [20, 6]. We consider these elements in Section 3. It will be seen that while these factors suggest a desired trend, a more concrete explanation of the odd conduction behavior is needed. We therefore focus our attention on the reorganization energy (RE). It turns out that the RE scheme fits best to the experimental observation. In the RE scheme, charge migrates from one monomer unit (see Fig 2) to another overcoming the activation energy barrier through thermal fluctuations.
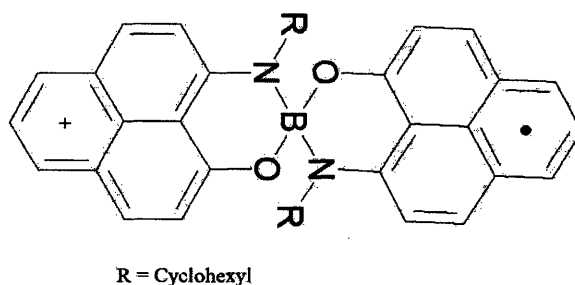

R = Cyclohexyl

Figure 1: cyclohexyl-substituted biphenalenyl radical [32].

5
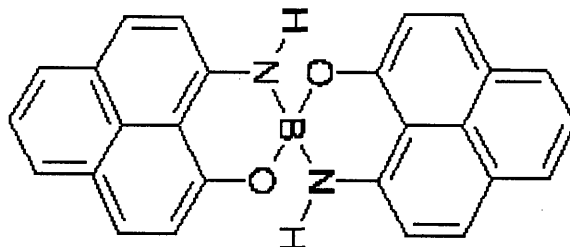
Figure 2: Spiro-biphenalenyl neutral radical molecule. This is one monomer unit of the dimer. Two monomers stack on top of each other to form a dimer.

2 Computational Methods

Other experimental and computational works [22, 25, 28, 38] have looked at effects of different alkyl groups attached to the nitrogen N. We keep H as the attached group, as we are investigating the general conduction mechanism as opposed to the effects of substructures on the conduction. To have a more detailed comparison of experimental and computational results, three levels of DFT are employed in this work: LDA, GGA, and hybrids. At each level of theory, the optimized geometry is obtained by successively optimizing geometries of the dimer that were built in the graphical interface, Gaussview. The optimized singlet dimer is shown in Fig.3. A larger basis set 6-311(d,p) is used to carry out subsequent single point calculations. We performed unrestricted DFT calculations for both the singlet and triplet states.
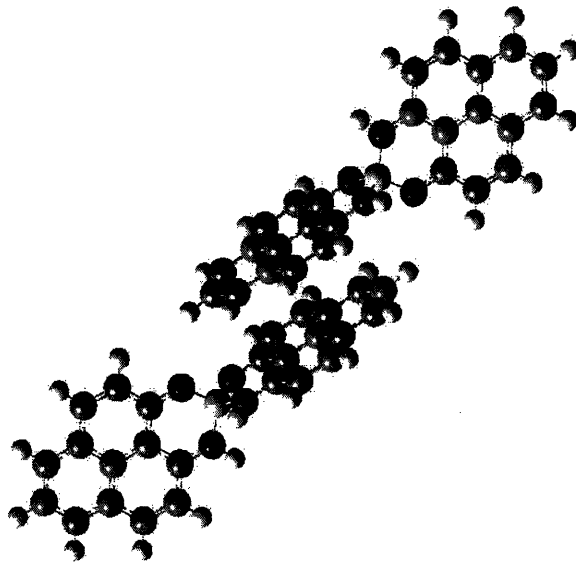
Figure 3: Spiro-biphenalenyl neutral radical dimer

3 Results and Discussion

3.1 Ground State Energy

From Table 1, we see that the energy difference between singlet and triplet states, $E_{sin} - E_{tri}$, are very small, in the order of 0.1 eV. The small difference from each functional calculation hints that singlet and triplet states are nearly degenerate, which is consistent with the experimental observation. We also see an interesting trend from Table 1, hybrid functionals (B3LYP, B98, and B1B95) give $E_{sin} - E_{tri} > 0$, whereas LSDA and GGA's (PW91 and PBE) give $E_{sin} - E_{tri} < 0$. It's generally believed that hybrid functionals are more accurate in predicting ground state energies [12], see also Appendix

7

5.2. According to Becke's argument [12], conventional LDA and GGA functionals use physically inappropriate exchange-correlation potential energy at the lower density limit. Hybrid functionals partially correct this problem by including a fraction (i.e. 0.20 in B3LYP) of the exact exchange into the total energy. However, since only like spins exchange, hybrid functionals correct relatively more exchange energy, E_x, of a triplet state than they do of a singlet state. As a result, one sees $E_{sin} - E_{tri} > 0$ from hybrid functionals and $E_{sin} - E_{tri} < 0$ from GGA functionals in Table 1.

Table 1: Energy differences between singlet and triplet states. Italic rows are results from geometry optimization calculations with 6-31G* basis set. Non-italic rows are results from single point calculations with basis set 6-311(d,p) at the B3LYP/6-31G* geometry.

Functional/Basis	$E_{singlet} - E_{triplet}$ (eV)
*LSDA/6-31G**	*-0.190*
*PW91/6-31G**	*-0.019*
*B3LYP/6-31G**	*0.218*
B3LYP/6-311(d,p)	0.218
B98/6-311(d,p)	0.190
PBE/6-311(d,p)	-0.027
B1B95/6-311(d,p)	0.136

3.2 Binding Energy and Intra-dimer Distance

Table 2 summarizes the geometric properties of singlet and triplet states. For optimized geometries, LSDA gives the shortest intradimer distances: 3.0Å for singlet state and 3.1Å for triplet state. LSDA is the only functional, among all the functionals used, that gives intradimer distances shorter than experimental X-ray data. LSDA distances are also the closest to experimental data of 3.2Å singlet and 3.3Å triplet. This can be attributed to the well known overbinding of LSDA functional as previously shown by others [16, 17]. The overbinding tendency of LSDA is also apparent from the comparison of binding energies, LSDA exhibits the highest binding energy in both singlet and triplet states. On the contrary, PW91 and B3LYP overestimate the intramolecular distance by about 10 percent. GGA functionals (PW91 and PBE) also bind the dimer. However, the results are much smaller than those obtained from LSDA. In addition, we found that B3LYP functional results in the smallest (even positive in the singlet case) binding energy among all functionals. Notice also that hybrid functionals in general give smaller binding energies than pure GGA functionals [14]. The same reasoning for $E_{sin} - E_{tri}$ in the previous paragraph holds valid in explaining the trend we observed here. Hybrid functionals relatively correct more exchange energy of the constituent monomers than they do of the dimer. Although our results show that the singlet state is more tightly bound and has shorter intra-dimer distance than the triplet state, the support seems weak when we compare with the experimental result, where the conductivity increases by as much

as two orders of magnitude in going from triplet state to singlet state. It is possible that the poor agreement is partly due to the difference in experimental and theoretical sample enviroment. For example, in the theoretical calculation, the Van der Waals interaction, which contributes to the binding energy, between each monomer is ignored. In addition, since we performed calculation on a single dimer, we also neglected crystal packing.

3.3 HOMO-LUMO gap

Generally, one regards HOMO and LUMO energy levels in organic semiconductors as analogous to valence and conduction energy bands respectively in inorganic semiconductors. The same analogy holds between the HOMO-LUMO gap and the band gap. Hence, smaller HOMO-LUMO gap corresponds to smaller band gap, which would generally make the crystal more conducting. Experimental transmittance spectra of a single ethyl-substituted crystal above and below the phase transition showed that the optical gap closes upon dimerization [25]. Furthermore, extended Hückel theory predicts that in the high temperature regime (T>100K, paramagnetic), the band gap is 0.23 eV, whereas it falls to 0.1 eV below the transition (T<100K, diamagnetic) [22]. As shown in Table 2 of our calculation, the HOMO-LUMO gaps from pure GGA functionals of the singlet state are about 0.13 eV, but the gaps from hybrid functionals are about three times larger, 0.44-0.51 eV. We suspect that the HOMO-LUMO gaps from pure GGA functionals were underestimated due to the derivative discontinuity problem in DFT [4, 5].

Hybrid functionals partially correct this problem and thus give rise to more accurate results. Singlet and triplet results are similar to within an order of magnitude for each given functional. In our study, we found that the HOMO-LUMO gap of the singlet state is smaller than that of the triplet state from all calculations with different functionals. This trend is consistent with the experiment [25] and Extended Hückel theory prediction [22]. However, contrary to the experimental results, there's little evidence of the closure of the HOMO-LUMO energy gap in the transition from the triplet to the singlet state in our calculations.

3.4 Charge localization

The passage of current through a crystal requires a pathway for the movement of electrons or holes. One way for the biphenalenyl molecular crystal to conduct current is to have the unpaired electrons located at the interior units of the dimer so that they can easily move from one monomer to another. This conduction mechanism is what Haddon et. al. had suggested. We summed the Mulliken atomic charges on both the interior and the exterior units of the dimer. As shown in Table 3, negative charges spread on both the interior and exterior units. Also, we noticed a trend that the interior unit is slightly more negatively charged than the exterior unit of the singlet state, on the contrary, the interior unit is slightly less negative than the exterior unit of the triplet state. From the DFT calculations, the differences between the two units are smaller than 0.1e for both paramagnetic and diamagnetic states. This result

weakly supports Haddon's conclusion: "in the paramagnetic state, unpaired electrons are located in the exterior phenalenyl units of the dimers, whereas in the diamagnetic state the electrons migrate to the interior phenalenyl units and spin pair as a π-dimer." [25] The Hartree Fock results show a much greater charge difference ($\sim$0.5e) between the interior and the exterior units. Nonetheless, the charge is still delocalized throughout the molecule in both states. Note that while DFT generally delocalizes the charge too much, Hartree Fock tends to do the opposite [23]. Although we can't firmly say that charge localization does not contribute to electrical conduction, it's only marginally convincing.

3.5 Reorganization energy

Because the simple proposals above do not fit the experimental observations, we seek the answer to the seemingly counter-intuitive experimental observation of conducting singlet state and insulating triplet state from the perspective of charge transfer reorganization energies. Other studies have suggested that a hopping mechanism is involved in the conduction of oligomers [31, 33]. We further explore this hopping scheme in the Biphenalenyl dimer. A hole transfer process between adjacent spatially separated molecules can be summarized as,

$$M1 + M2^{+} \rightarrow M1^{+} + M2 \tag{1}$$
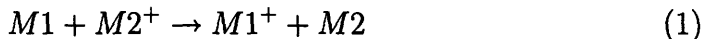
where M represents the neutral species undergoing charge transfer, and the M^{+} species contains the hole. A similar representation can be used in

Table 2: HOMO-LUMO gap (eV), binding energy (eV), and intramolecular distance (Å) of biphenalenyl molecule. Italic rows are results from geometry optimization calculations with 6-31G* basis set. Non-italic rows are results from single point calculations with basis set 6-311(d,p) at the B3LYP/6-31G* geometry.

	homo-lumo gap		Binding energy		Intra-dimer distance	
	Singlet	Triplet	Singlet	Triplet	Singlet	Triplet
LSDA	*0.21*	*0.32*	*-1.09*	*-2.18*	*3.0*	*3.1*
PW91	*0.13*	*0.10*	*-7.34*	*-0.22*	*3.5*	*3.7*
B3LYP	*0.44*	*0.65*	*0.16*	*-0.05*	*3.4*	*3.8*
B3LYP	0.44	0.64	0.27	0.01		
B98	0.47	0.86	0	-0.12		
PBE	0.13	0.12	-0.13	-0.11		
B1B95	0.57	0.74	-0.01	-0.13		

electrontransfer processes. One of the key parameters in a charge transfer process is the reorganization energy, λ, due to geometric relaxation. In a redox reaction, the RE is the energy required for all structural adjustments/reorganizations, which are needed in order that the acceptor and the donor assume the configuration required for the charge transfer. To illustrate the physical meaning of reorganization energy, we have represented in Fig.5 the potential energy surface (PES) of a hole transfer process of the type in Eq.1 and Fig.4. Immediately after the charge migrates from M1 to M2, M1 becomes neutral but with cation geometry (E_0^*), and M2 becomes a cation

Table 3: Comparison of charge localization from optimized geometries of LSDA, PW91, and B3LYP. Calculations are done with 6-31G* basis set

Functional	Interior (e)		Exterior (e)		Boron (e)	
	Singlet	Triplet	Singlet	Triplet	Singlet	Triplet
LSDA	-0.29	-0.23	-0.22	-0.28	0.51	0.51
B3LYP	-0.40	-0.31	-0.34	-0.42	0.74	0.74
PW91	-0.33	-0.29	-0.32	-0.36	0.66	0.65
HF	-0.87	-0.21	-0.28	-0.93	1.16	1.14

but with neutral geometry (E_+^*). Now both M1 and M2 are energetically unstable and will eventually relax to their equilibrium states, E_0 and E_+.
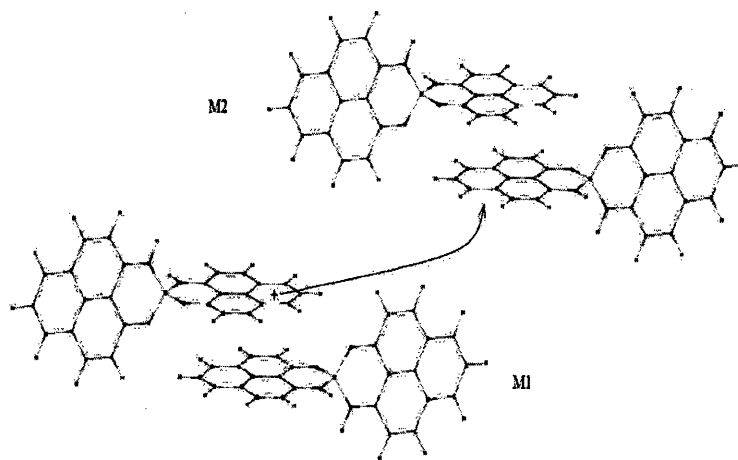

Figure 4: Inter-molecular hole transport

The charge transfer process can be divided into two steps. First, there is a vertical transition from the minimum of the neutral molecule to the cation
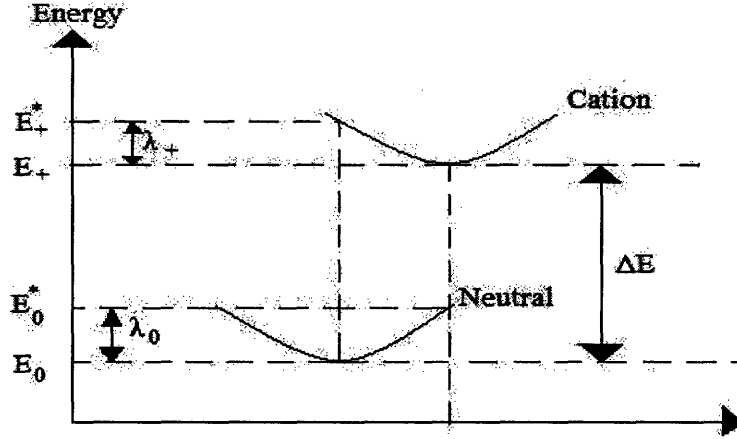
Figure 5: Potential energy curves of a hole transfer reaction as a function of various reorganization components $\lambda = \lambda_+ + \lambda_0$.

surface. The next step corresponds to the relaxation of the cation to its most favorable geometry. As seen in Fig.5, the reorganization energy consists of two terms:

$$\lambda_0 = E_0^* - E_0, \tag{2}$$

$$\lambda_+ = E_+^* - E_+, \tag{3}$$

The overall RE is the sum of these two terms, $\lambda_h = \lambda_0 + \lambda_+$, where subscript "h" indicates that holes are the charge transport carriers. In Fig.5, the electronic states E_0 and E_+ represent the energies of the neutral and cation species in their equilibrium geometries, while E_0^* and E_+^* represent the energies of the neutral and cation species with the geometries of the cation

and neutral species, respectively. Therefore, λ_0 is the energy required for the neutral system in its equilibrium geometry to adapt the cation geometry. Similarly, λ_+ is the energy required for the cation to adapt the geometry of the neutral system. ΔE is the adiabatic ionization energy of the molecule.

In a charge transfer process, the reorganization energy λ is closely linked to how fast the process occurs through Marcus theory and Arrhenius relationship. In Marcus theory, the activation energy for the charge transfer (the energy barrier hindering the hole to migrate from M1 to M2 in Fig 4), $\Delta G^{\ddagger}$, is given by

$$\Delta G^{\ddagger} = \frac{(\lambda + \Delta G^0)^2}{4\lambda},\qquad (4)$$

where ΔG^0 is the change in Gibb's free energy of reaction at normal conditions, which is zero for symmetric energy transfer. Eq.4 then can be used in the Arrhenius relationship for the rate constant:

$$k_{\mathrm{ET}} = A\exp(-\Delta G^{\ddagger}/k_{\mathrm{B}}T),\qquad (5)$$

where k_{B} is the Boltzmann constant. Eq.4 and Eq.5 can be applied to both singlet and triplet states of the neutral molecule as illustrated in Fig.5. In the singlet case, we denote the reorganization energy as λ^{sin} and charge transfer rate as k^{sin}. Similarly, in the triplet case, we have λ^{tri} and k^{tri}. By comparing Eq.4 and Eq.5, we see that if $\lambda^{tri} > \lambda^{sin}$, then $\mathrm{k}^{tri} < \mathrm{k}^{sin}$.

Reorganization energy were thus performed on optimized biphenalenyl dimer constrained at experimental distances. We held the intermolecular distance to experimental X-ray values: 3.2Å for singlet state and 3.3Å for triplet state. Furthermore, for charge constrained cation and anion calcula-

tions, we constrained the extra charge to one of the monomers in the dimer and then optimized the geometries. Similarly, for charge constrained singlet and triplet dimers, we put a positive charge on one monomer and a negative charge on the other, so that the net charge on the dimer is zero. This charge constrained geometry optimization procedure is made possible through the use of constrained DFT (CDFT) [34]. The key idea of CDFT is to obtain the particular external potential that has the constrained state as its ground state. Wu and Van Voorhis have shown that the same energy state that is the minimum with respect to the constraint is actually a maximum with respect to the constraint potential [34]. Inspired by the direct method for optimized effective potential (OEP) [26, 27], they've also established an efficient method to directly optimize the required potential by performing an unconstrained maximization to find the correct potential at each self-consistent iteration. This method gives the desired state and the required potential at convergence. CDFT is implemented in NWChem and is useful for our reorganization energy calculations. All charge constrained calculations were done with NWChem and all calculations without charge constraint were done with Gaussian03. For these calculations, we used B3LYP/6-31G* as functional/basis. It's important to note that we held the intra-molecular distance to the experimental X-ray values since the results from B3LYP geometry optimizations were over-estimated, as shown in Table 2. From Table 4, we see that for hole transport, $\lambda_h^{tri} > \lambda_h^{sin}$. This implies that $k^{tri} < k^{sin}$. In other words, the rate of hole transport is greater in the singlet case than in triplet, and hence singlet state is more conducting than

17

triplet state. Blom et. al. have demonstrated that in poly (p-phenylene vinylene) (PPV), the electron current is smaller than the hole current, and the hole mobility exceeds the electron mobility by more than an order of magnitude at room temperature [15, 21]. Hence, it's likely that holes are the conduction carriers. Interestingly, it appears to be the opposite, $\lambda_e^{tri} < \lambda_e^{sin}$, in electron transport. We postulate that the paramagnetic state would exhibit higher conductivity than the diamagnetic state, if electrons were the conduction carriers in biphenalenyl crystal, which might be achievable via doping and careful sample preparation. It is well known that organic conductors are p-type, in which electrons are trapped, and consequently, holes are the main conduction carriers [33]. We also considered the charge delocalized case, where the extra charge is equally distributed to both monomers in the dimer as opposed to being constrained to one monomer as in the charge localized case. Note that charge delocalized systems show the same trend as charge localized systems, $\lambda_h^{tri} > \lambda_h^{sin}$ and $\lambda_e^{tri} < \lambda_e^{sin}$. For charge localized systems, the difference between triplet and singlet state is slightly larger than that of charge delocalized systems, see Table 4. The unusual display of high conductivity in the singlet state can be understood as a consequence of the relatively high rate of hole transfer from one dimer to another.

4 Conclusion

We have undertaken a detailed analysis of the HOMO-LUMO gap, charge localization, and reorganization energy of the spiro-biphenalenyl neutral radical

18

Table 4: Inter-dimer reorganization energy of biphenalenyl molecule in eV

	Hole (eV)		Electron (eV)	
	localized	delocalized	localized	delocalized
Triplet	0.25	0.14	0.08	0.11
Singlet	0.18	0.03	0.22	0.33

dimer. We saw no significant difference in the HOMO-LUMO gap, or charge localization between singlet and triplet state dimers. The unusual conductivity increase in going from triplet to singlet state can be understood as a result of the higher reorganization energy in the charge transfer from triplet state to cation state, than in the charge transfer from singlet state to cation state. We conclude that the oddity of the insulating paramagnetic state and conducting diamagnetic state is mainly due to the higher rate of hole transport of the latter. However, we should point out that we performed calculation on the biphenalenyl dimer in its gaseous state rather than solid state. More complete understanding of the conduction mechanism will require further experimental and theoretical work. It is worth noting that our geometry optimization method did not provide the correct inter-monomer distance. Reorganization energy were thus performed on optimized biphenalenyl dimer constraining at experimental distance. More sophisticated methods are needed for geometry optimization that gives accurate inter-monomer distance.

5 Appendix

Density functional theory (DFT) is an accurate, rigorous and popular method for solving many-body problems in quantum chemistry and solid-state physics [1, 2]. DFT has successfully predicted many useful properties of atoms, molecules, and solids [9]. It is also useful in industry for the design of materials, reactions, pharmaceuticals and molecular dynamics [18]. In DFT, chemical and physical properties are studied from the perspective of looking at the electron densities rather than the many-body wave-function. Most modern density functional calculations involve solving the Kohn-Sham equations for a set of N orbitals. In principle, the sum of these orbitals' densities equals the exact ground-state density, from which the ground-state energy can be extracted. The exchange-correlation energy, $E_{xc}[n]$, accounts for a critical part of the ground state energy, and is the main focus of this work.

We propose a new hybrid density functional, which incorporates (a high percentage of) exact exchange, Meta-GGA exchange correlation, and correlation from second order perturbation theory. We describe in details the motivation behind the present work. We investigate the success and shortcomings of this functional by applying it to calculations of atomization energies of the G1 set, binding energies of Van der Waals complexes, and reaction barrier heights. We present the performance of this functional by comparing our results to those of other well established GGA, meta-GGA, and hybrid functionals.

5.1 Kohn-Sham Equation vs. Schrödinger Equation

In quantum mechanics, the time independent Schrödinger equation is expressed as

$$\hat{H}\Psi_i(\mathbf{x_1}, \mathbf{x_2}, ..., \mathbf{x_N}) = E_i\Psi_i(\mathbf{x_1}, \mathbf{x_2}, ..., \mathbf{x_N}), \qquad (6)$$

where $\hat{H}$ is the Hamiltonian operator and $\Psi_i(\mathbf{x_1}, \mathbf{x_2}, ..., \mathbf{x_N})$ is the many-particle wavefunction. If we apply the Born-Oppenheimer approximation, which states that the motion of the Nuclei is much slower than that of the electrons, we have the Hamiltonian operator that looks like

$$\hat{H} = -\frac{1}{2}\sum_{i=1}^{N}\nabla_i^2 - \sum_{i=1}^{N}\sum_{A=1}^{M}\frac{Z_A}{r_{iA}} + \sum_{i}^{N}\frac{1}{r_{ij}} = \hat{T} + \hat{V}_{Ne} + \hat{V}_{ee} \qquad (7)$$

where the first term is the kinetic energy term, the second term is the nuclear attraction term, and the last term is the inter-electronic repulsion term. It is the last term that scales factorially, and thus makes the Schrödinger equation difficult to solve accurately.

On the other hand, the Kohn-Sham equation avoids solving the many-body wave-functions directly. Instead, Kohn-Sham equation involves only one-particle wave-functions that give the same density as the ground state density of the real system. Eq.8 below is the Kohn-Sham equation,

$$\{-\frac{1}{2}\nabla^2 + v_S(r)\}\phi_i(r) = \epsilon_i\phi_i(r), \qquad (8)$$

where the first term is the kinetic energy operator, the second term is the effective potential, and $\phi_i(r)$ is the Kohn-Sham orbital of a single particle. The potential energy term can be decomposed into three parts,

$$v_S(r) = \int\frac{n(r_2)}{r_{12}} - \sum_{A}^{M}\frac{Z_A}{r_{1A}} + v_{xc}(r_1), v_{xc}(\mathbf{r}) = \frac{\delta E_{xc}[n]}{\delta n(\mathbf{r})} \qquad (9)$$

In Eq.9, the first piece is the Hartree potential, the second piece is the nuclear attractive potential, and the last piece is the exchange-correlation potential. The exchange-correlation energy can be viewed as the Coulomb interaction between the charge density and its surrounding exchange-correlation hole. Both the Hartree and the nuclear attraction potentials can be expressed as an explicit functional of the electron density, n. However, the exact form of the exchange-correlation functional E_{xc} is unknown, hence, must be approximated in DFT for the computation of electronic properties. This leads to our discussion of the levels of approximation to E_{xc} in the next section.

5.2 Motivation

According to Perdew et al. [29], the various steps forward in the development of more accurate density functionals can be assigned to various rungs of "Jacob's ladder." In that picture, the first rung of the ladder is the local density approximation (LDA); the second rung is the generalized gradient approxiamtion (GGA); the third rung is a hybrid functional; the forth rung is the meta-GGA functional; and our proposed functional is on the fifth rung, the hyper-hybrid functional. Here, we provide a brief description of each type of functional going up the Jacob's ladder. The LDA functional makes the assumption that all electron densities are uniform, and E_{xc} depends only on the density, n. It's a great approximation for metals, and has seen immense success in solid state physics. However, the fact that densities in atoms and molecules are non-uniform makes it a poor approximation for these systems.

Generalized gradient approximations (GGAs) take a step further by including the gradient of the density, ∇n, as a basic variable of $E_{xc}[n]$. Examples of GGA include PBE [13] and PW91 [10]. Going up a rung of the ladder, we have hybrid functionals. Hybrid functionals are obtained by mixing a fraction (with either empirical or non-empirical parameters) of the exact exchange energy into GGA $E_{xc}[n]$. An example of a hybrid with empirical parameters is the famous and popular B3LYP [12]; PBE0 [19] is an example of non-empirical hybrid. The next type, meta-GGA, sees advantage over GGA with the addition of kinetic energy density as a basic variable. The TPSS functional, which is the functional of interest in the present work, is a meta-GGA functional. Similar to but more advanced, and in many cases more accurate than hybrid functionals, are hyper-hybrid functionals. Hyper-hybrids have the ability to accomplish the "best of both worlds" since they have embedded in them both the exact exchange energy and the second order perturbation correlation energy. The equations below depict the unique features of each type of functional.

$$E_{xc}^{LDA}[n] = \int d^3 r n(\mathbf{r}) \varepsilon_{xc}^{unif}(n_\uparrow(\mathbf{r}), n_\downarrow(\mathbf{r})) \tag{10}$$

$$E_{xc}^{GGA}[n] = \int d^3 r n \varepsilon_{xc}(n_\uparrow, n_\downarrow, \nabla n_\uparrow, \nabla n_\downarrow) \tag{11}$$

$$E_{xc}^{hybrid} = E_{xc}^{GGA} + a_x(E_x^{HF} - E_x^{GGA}) \tag{12}$$

$$E_{xc}^{mGGA}[n] = \int d^3 r n \varepsilon_{xc}(n_\uparrow, n_\downarrow, \nabla n_\uparrow, \nabla n_\downarrow, \tau_\uparrow, \tau_\downarrow), \tag{13}$$

where

$$\tau_\sigma = \sum_i^{occup} \frac{1}{2} |\nabla \psi_{i\sigma}(\mathbf{r})|^2 \tag{14}$$

23

is the kinetic energy density for the occupied Kohn-Sham orbitals $\psi_{i\sigma}(\mathbf{r})$.

$$E_{xc}^{h.h.} = E_{xc}^{mGGA} + a_x(E_x^{HF} - E_x^{mGGA}) + b(E_c^{PT2} - E_c^{mGGA}) + c(E_c^{PT2} - lim_{\lambda \to 0} E_c^{mGGA}[n_\lambda])$$

$$(15)$$

The fifth rung of the Jacob's ladder, Eq.15, is what we're investigating.

The motivation behind mixing in exact exchange lies in the adiabatic connection formula,

$$E_{XC} = \int_0^1 U_{XC}^\lambda d\lambda, \tag{16}$$

where λ is an interelectronic coupling-strength parameter that "switches on" the $1/r$ Coulomb repulsion between eletrons, and U_{XC}^λ is the potential energy of exchange-correlation at intermediate coupling strength λ. The system is the non-interacting Kohn-Sham system at $\lambda = 0$, and fully interacting real system at $\lambda = 1$. Eq.16 conncets the Kohn-Sham system to the real system through coupling strength integration. This coupling strength integration, which via the Feynman-Hellman theorem, incorporates the kinetic contribution of the correlation, T_c into a potential energy term. At the lower limit $\lambda = 0$, $U_{XC}^{\lambda=0}$ represents the exact exchange, i.e. $U_{XC}^{\lambda=0} = U_X$. Becke [12] argued that conventional LSDA and GGA functionals use physically inappropriate U_{XC}^λ near the $\lambda = 0$ limit. Thus, even very sophisticated GGA functionals suffer from the flaw of overbinding. Hybrid functionals partially correct this problem by including a fraction (i.e. 0.20 in B3LYP) of the exact exchange into the total energy. We take advantage of this partial lower limit $\lambda = 0$ correction by including some exact exchange energy into our proposed functional.

Now let's describe the reason for including the second order correlation $E_c{}^2$ into the proposed energy functional. Görling and Levy have developed a perturbation theory (GLPT) [11] for the correlation with respect to the coupling constant, λ,

$$E_c[n_\lambda] = e_{c,2}[n] + \lambda e_{c,3}[n] + \lambda^2 e_{c,4}[n] + ... \qquad (17)$$

They have shown that the high denisty limit (low λ limit) of the correlation energy, $lim_{\lambda \to 0} E_c[n_\lambda]$, can be explicitly expressed as the following *second-order* result,

$$lim_{\lambda \to 0} E_c[n_\lambda] = e_{c,2}[n] = \sum_{k=1}^{\infty} \frac{|<\Psi^0| \sum_{i=1}^{N} [u(r_i) + v_x(r_i)] |\Psi_k^0>|^2}{E^0 - E_k^0} \qquad (18)$$

This term is the long-range electron correlation that's responsible for dispersive (i.e. Van der Waals) interactions. It contains virtual KS orbitals (characteristic of the fifth rung of Jacob's ladder), which are missing in current GGAs and meta-GGAs. These virtual orbitals allow electron motion to be correlated when the two-electron operator is introduced, by giving the electrons the opportunity to move away from each other [35]. With the presence of $lim_{\lambda \to 0} E_c[n_\lambda]$ in our proposed functional, we hope to be able to describe Van der Waals interactions to higher accuracy.

Table below shows that E_c^{dfa} works well, this agrees with the common claim that approximate functionals work best at the $\lambda = 1$ end. The E_c^2 piece is too big, in other words, (1-a) is too big, and thus higher order terms were scaled down by too much. This perhaps could be improved if we scale up higher order terms, since E_c has the following form according to Görling-Levy perturbation theory.

$$E_c[n_\lambda] = e_{c,2}[n] + \lambda e_{c,3}[n] + \lambda^2 e_{c,4}[n] + ... \qquad (19)$$

$$E_c^\lambda = E_c[\frac{\rho}{\lambda^3}, \frac{\nabla\rho}{\lambda^4}] \qquad (20)$$

$$E_{c,\lambda} = \frac{d}{d\lambda}(\lambda^2 E_c^\lambda) = 2\lambda E_c^\lambda + \lambda^2 \frac{dE_c^\lambda}{d\lambda} \qquad (21)$$

In the high density limit,

$$\frac{dE_{c,\lambda}}{d\lambda}|_{\lambda=0} = 2E_c^\lambda|_{\lambda=0} = 2E_c^{(2)} \qquad (22)$$

5.3   Theoretical Details

We used the meta-GGA TPSS [29] functional for the E_{xc}^{mGGA} in Eq.15. TPSS functional is self-correlation free, and thus is desirable for systems containing hydrogen. First, TPSS Kohn-Sham (KS) orbitals of the G1 set molecules (shown in Table 1) were generated using Gaussian03 and NWChem. Then, we used KS orbitals to calculate individual terms in Eq.15. We optimized the parameters a_x, b, and c in Eq.15 iteratively for the atomization energies of the G1 molecules. At convergence, we obtained a set of best fit parameters. We then put these parameters back into Eq.15 to calculate barrier heights and Van der Waals binding energies. We used cc-pcvqz basis set [39] for atomization energy and barrier height calculations and cc-pvtz basis set [39] for Van der Waals interaction calculations.

5.4 Analysis

The coefficients we found from optimizing against the G1 set atomization energies are $a_x=0.67$, $b=0.24$, and $c=0.13$. The mean absolute error (MAE) from atomization energy is 2.10 kcal/mol. It's slightly better than B3LYP result, and much better than TPSSh [30] result, as shown in Table 5. We see better improvements in reaction barrier height calculations [36] in Table6. The results from the new hyper-hybrid are much better than both B3LYP and TPSSh results. As expected, the proposed functional gives substantially smaller errors than existing hybrids of GGA and meta-GGA. This is manifest from the comparison [37] in Table 7.

Table 5: Comparison of mean absolute errors (in kcal/mol) of atomization energies of different functionals

	Proposed	B3LYP	TPSSh
MAE	**2.10**	2.21	4.51

Table 6: Comparison of mean absolute errors (in kcal/mol) of barrier heights of different functionals

	Proposed	B3LYP	TPSSh
MAE	**3.25**	4.28	6.32

Note that we used Kohn-Sham orbitals to calculate the PT2 correlation. The Kohn-Sham orbitals themselves have no physical significance besides the relation, $\epsilon_{HOMO} = -I$, where ϵ_{HOMO} is the energy of the highest occupied molecular orbital and I is the ionization energy. It's fascinating to see

Table 7: Comparison of mean absolute errors (in kcal/mol) of Van der Waals binding energies of different functionals

	Proposed	PBE0	TPSSh
Rare-Gas Dimer	**0.055**	0.099	0.113
Alkaline-Metal and Zn2	**0.694**	1.89	2.16
Zn-Rare-Gas Dimer	**0.078**	0.118	0.147

how inclusion of virtual KS orbitals enables one to calculate Van der Waals interaction to a much higher accuracy.

5.5 Remarks

Based on the physical ground of perturbation theory, we have climbed to the current top rung of the Jacob's ladder. The "best of both worlds", namely, the exact exchange and second order perturbation correlation energies are proven to be essential in aspects of thermochemistry such as atomization energy, reaction barrier height, and most notebly Van der Waals interaction. It will be interesting to see how well the proposed functional performs on systems with extended $\pi - \pi$ interactions such as the biphenalenyl radical dimer. More importantly, a further step can be taken to investigate more accurate treatment of excited states in DFT without having to resort to time-dependent DFT (TDDFT). The performance of present time non-TDDFT on excited states is shown in Fig.6.
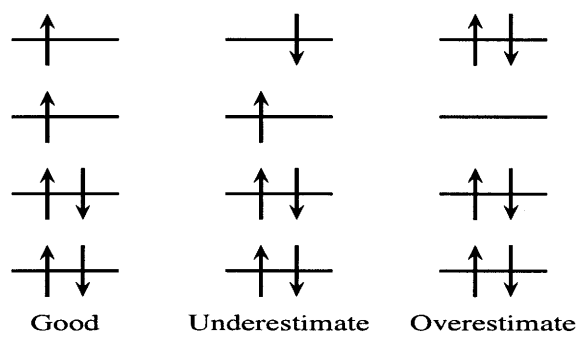
Figure 6: current performance of DFT on excited states

References

[1] Hohenberg, W. Kohn, Phys. Rev. **136**, B 864 (1964).

[2] W. Kohn, L. J. Sham, Phys. Rev. **140**, A1133 (1965).

[3] R. C. Haddon, Nature **256**, 394 (1975).

[4] J. P. Perdew, R. G. Parr, M. Levy, J. L. Balduz Jr, Phys. Rev. Lett. **49** 1691 (1982).

[5] J. P. Perdew, M. Levy, Phys. Rev. Lett **51** 1884 (1983).

[6] D. B. Cotts, Z. Reyes, *Electrically Conductive Organic Polyers for Advanced Applications*, Chapter 7 and 8, William Andrew Publishing/Noyes (1986).

[7] A. D. Becke, Phys. Rev. A **38** (6), 3098 (1988).

[8] C. Lee, W. Yang, R. G. Parr, Phys. Rev. B **37** (2), 785 (1988).

[9] R. O. Jones, O. Gunnarsson, Rev. Mod. Phys. **61**, 689 (1989).

[10] J.P. Perdew, J.A. Chevary, S.H. Vosko, K.A. Jackson, M.R. Pederson, D.J. Singh and C. Fiolhais, Phys. Rev. B **46**, 6671 (1992).

[11] A. Görling, M. Levy, Phys. Rev. B **47** 13105 (1993).

[12] A. D. Becke, J. Chem. Phys. **98**, 5648 (1993).

[13] J. P. Perdew, K. Burke, and M. Ernzerhof, J. Chem. Phys. **105** (22), 3865 (1996).

[14] J. P. Perdew, M. Ernzerhof, and K. Burke, Phys. Rev. Lett. **77**, 3865 (1996).

[15] P. W. M. Blom, M. J. M. de Jong, J. J. M. Vleggaar, Appl. Phys. Lett. **68** (23) 9982 (1996).

[16] D. C. Patton, D. V. Porezag, M. R. Pederson, Phys. Rev. B **55** (12) 7454 (1997).

[17] R. J, Deeth, H. D. B. Jenkins, J. PHys. Chem. A **101** (26) 4793 (1997).

[18] E.J. Baerends, O. V. Gritsenko, J. Phys. Chem. A **101**, 5383 (1997).

[19] C. Adamo and V. Barone, J. Chem. Phys. **110**, 6158 (1998).

[20] Conducting Polymers: Nobel Prize in Chemistry, 2000, Current Science **79** (12) (2000)

[21] H. C. F. Martens, J. N. Huiberts, P. W. M. Blom, Appl. Phys. Lett. **77** (12) 1852 (2000).

[22] X. Chi, M. E. Itkis, K. Kirschbaum, A. A. Pinerton, R. T. Oakley, A. W. Cordes, R. C. Haddon, J. Am. Chem. Soc **2001** (123) 4041 (2001).

[23] a. Dkhissi, D. Beljonne, R. Lazzaroni, F. Louwet, L. Groenendaal, J. L. Brédas, Int. J. Quant. Chem. **91** (3) 517 (2002).

[24] X. Chi, M. E. Itkis, R. W. Reed, R. T. Oakley, A. W. Cordes, R. C. Haddon, Science, **106** (33), 8278 (2002).

[25] M. E. Itkis, X. Chi, A. W. Cordes, R. C. Haddon, Science, **296** (5572), 1443 (2002).

[26] W. Yang, Q. Wu, Phys. Rev. Lett **89** 143002 (2002).

[27] Q. Wu, W. Yang, J. Theo. Comp. Chem **2** (4) 627 (2003).

[28] J. S. Huang, M. Kertesz, J. Am. Chem. Soc. **125** (44), 13334 (2003).

[29] J. Tao, J. P. Perdew, V. N. Starovenov, G. E. Scuseria, Phys. Rev. Lett **91**, 146401 (2003).

[30] V. Staroverov, G. Scuseria, J. Tao and J. Perdew, J. Chem Phys. **119**, 12129 (2003).

[31] J. Bredas, D. Beljonne, V. Coropceanu, J. Cornil, Chem. Rev. **104**, 4971 (2004).

[32] S. K. Pal, M. E. Itkis, F. S. Tham, R. W. Reed, R. T. Oakley, R. C. Haddon, Science **309**, 281 (2005).

[33] G. R. Hutchison, M. A. Ratner, T. J. Marks, J. Am. Chem. Soc. **127** 2339 (2005).

[34] Q. Wu, T. Van Voorhis, Phys. Rev. A **72** 024502 (2005).

[35] R. J. Bartlett, V. F. Lotrich, I. V. Schweigert, J. Chem. Phys. **123**, 062205 (2005).

[36] Y. Zhao, D. G. Truhlar, J. Phys. Chem. A **109**, 2012 (2005).

[37] Y. Zhao, D. G. Truhlar, J. Phys. Chem. A **110**, 5121 (2006).

[38] J. S. Huang, M. Kertesz, J. Am. Chem. Soc. **128** (5), 1418 (2006).

[39] Information on basis set: http://www.emsl.pnl.gov/forms/basisform.html